Cardiovascular Research (2012) **94**, 48–57
doi:10.1093/cvr/cvr357

Heterogeneous atrial wall thickness and stretch promote scroll waves anchoring during atrial fibrillation

Masatoshi Yamazaki[1,2], Sergey Mironov[1], Clément Taravant[1], Julien Brec[1], Luis M. Vaquero[3], Krishna Bandaru[1], Uma Mahesh R Avula[1], Haruo Honjo[2], Itsuo Kodama[2], Omer Berenfeld[1], and Jérôme Kalifa[1]*

[1]Center for Arrhythmia Research, Department of Internal Medicine, University of Michigan, 5025 Venture Drive, Ann Arbor, MI 48108, USA; [2]Research Institute of Environmental Medicine, Nagoya University, Nagoya, Japan; and [3]Telefonica I+D, Madrid, Spain

Received 7 June 2011; revised 22 December 2011; accepted 27 December 2011; online publish-ahead-of-print 6 January 2012

Time for primary review: 35 days

Aims Atrial dilatation and myocardial stretch are strongly associated with atrial fibrillation (AF). However, the mechanisms by which the three-dimensional (3D) atrial architecture and heterogeneous stretch contribute to AF perpetuation are incompletely understood. We compared AF dynamics during stretch-related AF (pressure: 12 cmH_2O) in normal sheep hearts ($n = 5$) and in persistent AF (PtAF, $n = 8$)-remodelled hearts subjected to prolonged atrial tachypacing. We hypothesized that, in the presence of stretch, meandering 3D atrial scroll waves (ASWs) anchor in regions of large spatial gradients in wall thickness.

Methods and results We implemented a high-resolution optical mapping set-up that enabled simultaneous epicardial- and endoscopy-guided endocardial recordings of the intact atria in Langendorff-perfused normal and PtAF (AF duration: 21.3 ± 11.9 days) hearts. The numbers and lifespan of long-lasting ASWs (>3 rotations) were greater in PtAF than normal (lifespan 0.9 ± 0.5 vs. 0.4 ± 0.2 s/(3 s of AF), $P < 0.05$). Than normal hearts, focal breakthroughs interacted with ASWs at the posterior left atrium and left atrial appendage to maintain AF. In PtAF hearts, ASW filaments seemed to span the atrial wall from endocardium to epicardium. Numerical simulations using 3D atrial geometries (Courtemanche-Ramirez-Nattel human atrial model) predicted that, similar to experiments, filaments of meandering ASWs stabilized at locations with large gradients in myocardial thickness. Moreover, simulations predicted that ionic remodelling and heterogeneous distribution of stretch-activated channel conductances contributed to filament stabilization.

Conclusion The heterogeneous atrial wall thickness and atrial stretch, together with ionic and anatomic remodelling caused by AF, are the main factors allowing ASW and AF maintenance.

Keywords 3D atrial structure • Atrial fibrillation • Atrial dilatation • Remodelling • Simulation

1. Introduction

Atrial fibrillation (AF), the most common arrhythmia in adults, affects more than 6 million Europeans/year.[1] Atrial stretch is known to be a major determinant of AF perpetuation, specifically after atrial remodelling.[2] However, the electrophysiological mechanisms of stretch-related AF in remodelled atria are incompletely understood.[3,4] In recent years, major mechanistic differences between paroxysmal AF and persistent AF (PtAF) maintenance have been highlighted. While the pulmonary veins (PVs) are the main region harbouring AF sources in paroxysmal AF patients, wider atrial regions including the inter-atrial septum, the atrial free walls, and the superior vena cava, have proved to be critical for PtAF maintenance.[5] In addition, radio-frequency ablation successes point towards a fundamental role of the three-dimensional (3D) atrial structure in AF perpetuation. For instance, transmural ablation lesions are considered to be a predictor of AF respite.[6] Thus, we endeavoured to investigate the electrophysiological mechanisms of AF in stretched atria that have been

* Corresponding author. Tel: +917 734 5014; fax: +1 315 464 8000, Email: kalifaj@umich.edu

previously remodelled by prolonged AF episodes. Using simultaneous epicardial- and endoscopy-guided[7] endocardial mapping in Langendorff-perfused sheep hearts and numerical simulations, we examined in detail the AF dynamics within the 3D atrial structure under conditions of myocardial stretch in normal hearts (NHs) and in hearts subjected to long-term atrial tachypacing. We hypothesized that atrial scroll waves (ASWs) and spontaneous impulses are formed in the complex atrial architecture and enable AF perpetuation. We focused exclusively on the formation of ASW with linear filaments (I-shaped) and postulated that filament tension and stability are determined by heterogeneous levels of myocardial thickness, specifically after ionic remodelling. The results presented describe 3D mechanisms of AF maintenance in normal and remodelled atria. They indicate how ASWs anchoring and stabilization within regions of sharp thickness gradients result in AF perpetuation.

2. Methods

2.1 Optical mapping

All animal experiments were carried out according to the University of Michigan Committee on Use and Care of Animals (Protocol Number: #no. 09963) and the National Institutes of Health guidelines.[8] Thirteen sheep (normal $n = 5$, PtAF $n = 8$, 45–50 kg) were anaesthetized with intra-venous bolus injection of propofol (5–10 mg/kg). Hearts were excised with vital organ removal under anaesthesia and Langendorff-perfused with warm oxygenated Tyrode's solution (pH 7.4; 95% O_2, 5% CO_2, and 36–38°C). After perforation of the intra-atrial septum, we sealed all venous orifices except the inferior vena cava for controlling the level of intra-atrial pressure to 12 cmH_2O. AF was induced by burst pacing at a cycle length (CL) of 10 Hz. And those AF episodes were sustained in both normal (80.0 ± 15.8 min) and PtAF (82.5 ± 38.5 min) in this study. The set-up includes three CCD cameras recording (*Figure 1*) from the epicardial right atrial and left atrial appendage (RAA, LAA) and either the endocardial LAA or posterior left atrium (PLA). The latter camera is connected to a cardio-endoscope introduced in the left atrium by trans-septal route as described previously.[7,9] As also described elsewhere,[10] a bolus injection of 15 mL Di-4-ANEPPS (10 mg/mL), enabled recording fluorescence changes from an area of ~3 cm^2 at 500 frames/s to obtain 5 s movies (80 × 80 pixels). To reduce motion artefacts, we added 10 μM blebbistatin to the perfusate. Movies of the PLA, LAA, and RAA together with bipolar electrograms of the LAA, left atrium-pulmonary vein (LA-PV) junction, RAA and coronary sinus (CS) made possible the characterization of the dominant frequency (DF) distribution.

2.2 Movies analysis: activation patterns and dynamics

Simultaneous endocardial and epicardial movies were analysed on a wave-by-wave basis as follows: DF maps were obtained for each optical movie after applying a Fast Fourier Transformation of the fluorescence signal recorded at each pixel. To analyse wavebreaks location and rotor dynamics, we also constructed phase movies after a phase analysis according to Gray *et al.*[11] but modified as to be based on Hilbert transformation as in Warren *et al.*[12] For LAA views, a representative simultaneous endocardial–epicardial 1 s-movie sample for each animal was analysed during AF. After that, we obtained a DF map of the 1-second epoch

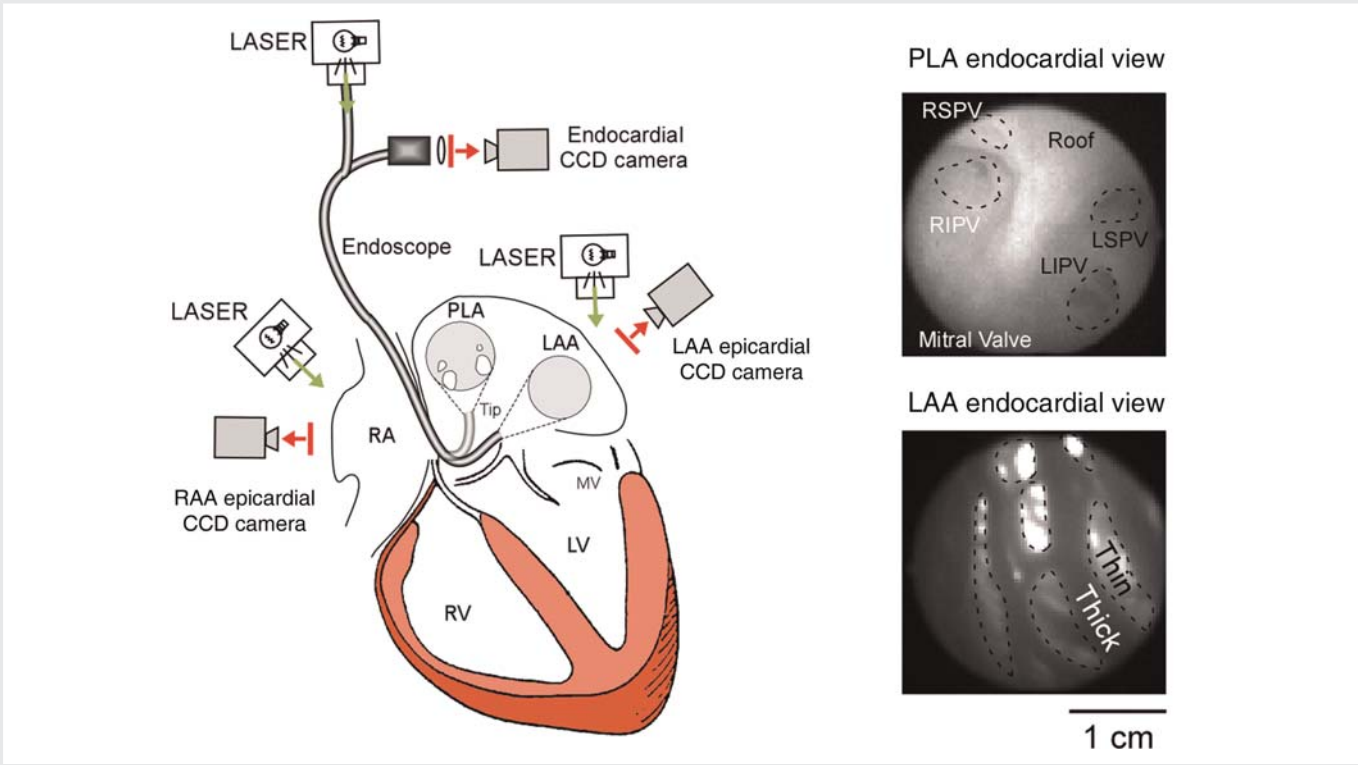

Figure 1 Optical mapping experimental set-up. A 3-CCD camera optical mapping set-up was implemented to acquire high-resolution movies of the atrial endocardium and epicardium. One of the CCD cameras was connected to an endoscope which tip could be directed towards the PLA or the LAA. Additionally, background pictures of the endocardial (right panels) or epicardial (not shown) anatomy could be obtained with a corresponding camera field-of-view.

analysed, we delineated the DF maximum (DFmax) region as follows: the pixels corresponding to a contiguous highest DF value ± 0.5 Hz were included in the DFmax region, which boundaries were drawn digitally. Thereafter, the corresponding phase movie was analysed with specific attention to wave patterns within the DFmax region. (i) Rotors, defined as a spiral wave rotating around an organizing centre for more than one rotation; (ii) breakthroughs (BTs), *Appearance:* wave, which observed after a 12 ms lifespan (six frames) locates within the field-of-view, i.e. which outer limits have no contact with the edges of the field-of-view but are at least in part intersecting with the DFmax region. *Propagation:* In general, BTs propagated centrifugally in a homogeneous manner; however, some BTs preferentially propagated in one direction. (iii) One-way propagation waves (OPs), waves emerging from one edge of the field, or in contact with the field-of-view edges within 12 ms of lifespan, and propagating in one direction throughout the field-of view including the DFmax region. Then, the epicardial and endocardial patterns were compared and the following groups were formed: (i) identical endocardial–epicardial wave activation: (a) dual endocardial–epicardial rotor: when the endocardial and epicardial reentrant activities where similar in terms of singularity point(s) anatomical locations, chirality (wavefront within 90° of each other) and CL (± 2 ms), the patterns were classified as an I-shaped filament atrial scroll wave (I-ASW). ASW is classically described as a 3D functional reentrant activity spanning through the full myocardial thickness. Depending on the shape of the centre of rotation (filament), the scroll wave may be described as I-shaped, U-shaped, and L-shaped[13] (b) 'endocardial–epicardial similarity in wave directionality': directionality was classified as identical when, besides similar wave morphologies on the epicardium and the endocardium, the endocardial–epicardial wave main directionality was similar. For example, when a wave was propagating from the upper to lower edge on the endocardium, a similar wave direction—upper edge to lower edge—was required to classify this wave as identical (c) 'endocardial–epicardial BTs': endocardial and epicardial BTs were classified as simultaneous when they appeared within 12 ms (six frames). (ii) Non-identical endocardial–epicardial wave activation: when epicardial and endocardial patterns were different in terms of pattern morphology and/or wave directionality we classified endocardial–epicardial patterns into the following wave patterns combinations: rotor-OPs, rotor-BTs, OP-BTs, OP-OPs of different direction. Additional classification criteria pertaining to cut-off values are presented in the Supplementary material online.

2.3 PtAF models

To obtain PtAF ($n = 8$), we employed an atrial tachypacing-induced PtAF model in sheep. PtAF sheep were anaesthetized with intra-venos propofol 4–6 mg/kg and isoflurane 1–3%. A right atrial pacing lead was implanted from right jugular vein at the RAA. To monitor the adequacy of anaesthesia, heart rate, respiratory rate, blood pressure, and body temperature were monitored during surgery. After 24 h of pace maker implantation, stimulation was initiated at 20 Hz in 30 s-periods. The stimulator automatically switched to a sensing mode once AF was detected, enabling AF to perpetuate in the absence of external stimulation. In all hearts, sustained AF episodes (21.3 ± 11.9 days) were obtained within 1–7 weeks of atrial tachypacing (see Supplementary material online, *Table S5*). Electrocardiogram (ECG) and echocardiography performed weekly indicated the presence of PtAF and of progressive atrial dilatation (see Supplementary material online, *Figure S1* and *Table S2*).

2.4 Numerical simulations

We conducted simulations using a 3D atrial geometries composed of two discs implemented with a human atrial model (Courtemanche-Ramirez-Nattel model).[14] We employed a rectangular volume including 100 × 100 × 50 nodes homogenously distributed and corresponding to 10 × 10 × 5 mm, some of them being active while others were dormant (*Figure 6A*). Control and PtAF conditions were mimicked by modifying three or four major ionic conductances as previously reported.[15] The 'AF-3 current condition' was obtained by incorporating a downregulation in the densities of the transient outward K^+ current, I_{to} (by 50%), the ultrarapid-delayed rectifier K^+ current, I_{Kur} (by 50%), and the L-type Ca^{2+} current, I_{CaL} (by 70%), without additional increase in the density of the inward rectifier K^+ current, I_{K1}. The 'AF-4 current condition' was obtained by associating an increase in I_{K1} density (by 100%) to the three aforementioned current changes. Also, two levels of stretch-activated channel conductances (thin: 4 μm, thick: 2 μm) were incorporated according to Kamkin *et al.*[16] A detailed description of the computer model, including the implementation of stretch-activated channels conductances, as well as the analyses performed is included in the *Figure 6* and Supplementary material online.

2.5 Statistics analysis

Group data were expressed as mean ± SD. Frequency data (*Figure 2C*) were compared with a repeated measure two-way analysis of variance test: 2 (condition; NH and PtAF) × 4 (location; LA-PV junction, LAA, RAA, and CS). Statistical comparisons in the constant pacing: (i) conduction velocity, (ii) action potential duration, (iii) wavelength was also performed by one-way ANOVA. Differences were considered significant when $P < 0.05$.

3. Results

3.1 AF dynamics associated with atrial stretch

We generated phase movies to examine global AF dynamics in the presence of stretch. In *Figure 2A*, we present representative phase maps obtained simultaneously from three different atrial locations at two different times during a long AF episode (top, 40 ms; bottom, 742 ms) in a PtAF heart. A clockwise rotor on the LAA epicardium (epi) lasted longer than 2 min. Importantly, in this experiment, long-lasting rotors (>3 rotations) appeared intermittently at the same epicardial location for the duration of the experiment (3–4 h). Simultaneously, the activity on the endocardium (endo) of the PLA was somewhat slower but very complex, manifesting as multiple BTs and wavebreaks (middle panel). However, on the RAA epicardium, the maps demonstrated relatively slow, spatio-temporally organized activity, including brief periods of figure-of-eight reentry (upper panel) and organized waves entering from outside the optical field. As shown by the top maps of *Figure 2B*, such global dynamics gave rise to a relatively shallow LAA-PLA-RAA DF gradient of 1.3 Hz, which indicated that the rotor in the LAA was the driver that maintained AF. By comparison, in an NH, the activity was maintained by a small source on the PLA-endo near the left PV. The DF of that source was 16 Hz, which resulted in a very steep PLA-LAA-RAA gradient of 9.6 Hz. Altogether, as summarized diagrammatically in *Figure 2C* and *D* analysis of the optical and/or electrical DF on four different locations (LA-PV junction, CS, LAA, and RAA) demonstrated that in NHs, the PLA had the largest frequencies of activation, with relatively large gradients from LA to RA. However, in PtAF hearts, DFs were slower and the DF gradient was shallower. In other words, the overall DF dispersion was significantly larger in NH than PtAF hearts (8.7 ± 1.5 vs. 3.0 ± 1.0 Hz, $P < 0.05$). These results are very similar to those found previously in patients and indicate that atrial remodelling in PtAF somehow increases the ability of both atria to harbour AF sources away from the PVs.[5,17] *Figure 2E*, in five NHs, only a few non-sustained rotors confined to the PLA were

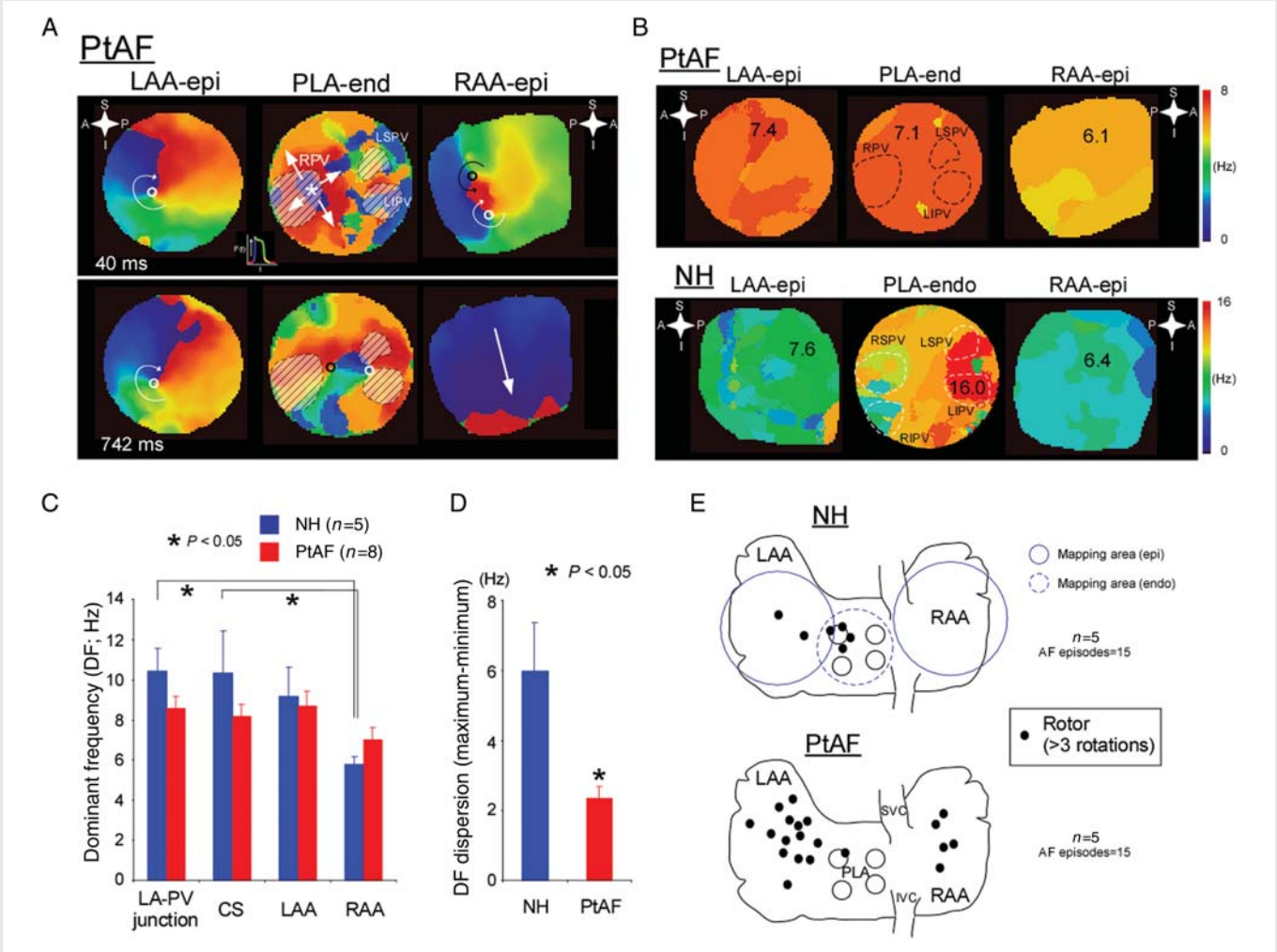

Figure 2 Reentry dynamics associated with atrial stretch. (*A*) Representative colour phase maps from three different locations in a PtAF heart. Left, clockwise rotor (curved white arrow) on epicardium of LAA (LAA-epi); middle, breakthrough (BT) (white star and arrows) and complex activation on the endocardium of the PLA (PLA-endo); right, figure-of-eight reentry (black and white circles) and one-way propagating waves (white arrow) on epicardium of the right atrial appendage (RAA-epi). Each colour corresponds to a different phase of the action potential (see insert between top LAA-epi and PLA-end maps). (*B*) Representative DF maps from same experiment as in (*A*). Numbers and colours are in Hz. (*C*) DFs at the LA-PV junction, CS, LAA and RAA during stretch-related AF in NH and PtAF hearts. (*D*) DF dispersion (DFmax-minimum) in NH and PtAF hearts. (*E*) Diagrams of the atria showing locations of epicardial rotors (black dots, >3 rotations) in NH (top) and PtAF (bottom) hearts. The areas mapped by the three-camera set-up are represented by the blue circles on the top diagram (plain for epicardial and dashed for endocardial).

seen during AF. In sharp contrast, in five PtAF, hearts rotors lasting >3 rotations were found in higher numbers and with much wider distribution throughout both atria, although with some preference for the LA.

3.2 Activation patterns of stretch-related AF at the LAA

In the NH, AF was characterized by multiple centrifugal BTs, wavebreaks and short-lived reentries suggesting an interplay between reentrant waves and fibrillatory waves conducted transmurally as previously reported.[9] *Figure 3* summarizes the overall differences in patterns of propagation that were observed at the regions with the highest LAA DF. In average number of activation in NH and PtAF, I- ASW was significantly increased from 1.0 $\pm$ 1.4 to 6.2 $\pm$ 2.3 ($P <$ 0.05), whereas BTs number was significantly decreased from 3.8 $\pm$ 1.6 to 0.2 $\pm$ 0.4 ($P < 0.05$). The patterns of propagation were classified as indicated on the lower schematic. As depicted in the graphs, the vast majority of LAA patterns was constituted by I-ASWs (31/42 AF waves) in PtAF hearts, while BTs (19/43 AF waves) and one-way propagations (13/43 AF waves) were the most frequent in NHs.

3.3 AF sources and 3D scroll waves

We hypothesized that the atrial rotors recorded optically from the epicardium of PtAF and NHs corresponded to 3D scroll waves spanning the thickness of the wall. Therefore, we obtained simultaneous epicardial- and endoscopy-guided endocardial movies to reconstruct 3D ASWs associated with AF. Phase maps of the two recording surfaces of a given atrial area made it possible to detected concurrent epi and endo phase singularities (PSs) around which functional reentry organized (see Supplementary material online). As illustrated in

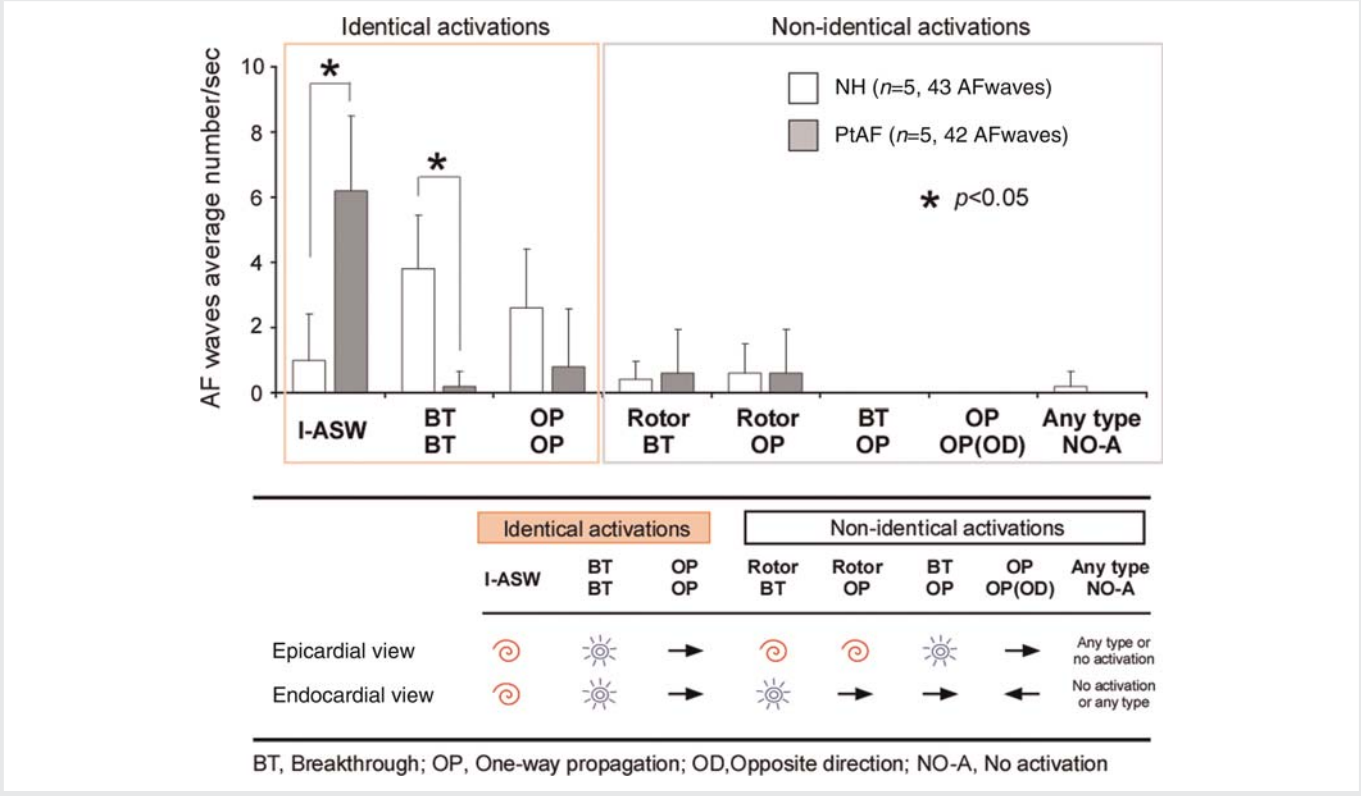

Figure 3 LAA 3-D activation patterns during AF in normal (NH) and persistent AF (PtAF) hearts. (Upper panel) Most of the patterns were identical on the pericardium and the endocardium (86%). In PtAF hearts, a high percentage of I-ASWs was seen whereas in normal hearts (NH), it exhibited a large portion of patterns that were BTs and one-way propagation waves. (Lower panel) Classification of endocardial and epicardial AF patterns.

Figure 4, analysing the synchronous dynamics of epi and endo rotors of the same frequency and chirality made it possible to connect their respective PSs by means of a virtual filament, which then was used to follow the dynamics of the resulting ASW. *Figure 4A* and Supplementary material online, *Movie S1* illustrate the behaviour of a long-lasting ASW with an I-shaped filament (white line) on the LAA. The rotation was clockwise and sequential snapshots taken over a period of 1120 ms demonstrated that the filament meandered over a relatively narrow area. In addition, similar to what has been shown for scroll waves in other excitable media,[18,19] the epicardial and endocardial ends of the filament could be in phase or else show phase shifts relative to each other (e.g. middle panels) that may have resulted in filament twist. In *Figure 4B*, the epi and endo singularity points' pixel coordinates were utilized to trace their trajectories with respect to the real anatomy of the LAA. This allowed estimating the filament's drift trajectory and its interaction with the atrial wall. For example, *Figure 4C* and Supplementary material online, *Movie S2* indicate that the ASW shown in *Figure 4A* and *B* was organized by a filament that drifted along the edge of a large pectinate muscle (white line).

3.4 Short-lived phase singularity vs. long-lasting scroll waves

Figure 5A shows sequential epicardial phase maps of the LAA of an NH (top) and a PtAF heart (bottom). In the NH, AF was characterized by multiple centrifugal BTs, wavebreaks, and short-lived reentries suggesting an interplay between reentrant and spontaneous focal discharge mechanisms.[9] In contrast, the three sequential phase maps from a PtAF heart are all highly organized by a single, relatively stable rotor. *Figure 5B* summarizes the phase singularity (top, red dots) and I-filament ASW (bottom, blue dots) distributions of two normal and three PtAF hearts during 1000 ms, superimposed on the anatomy of the LAA. Multiple short-lasting PSs formed and rapidly disappeared in NHs, while in PtAF hearts most PSs evolved into I-filament ASWs. In the NHs, PSs distributed widely throughout the LA structure, while only a couple of PSs evolved into I-filament ASWs lasting more than three rotations. In PtAF hearts, the vast majority of the PSs evolved into long-lasting ASWs. Analysis of the ASWs/PSs lifespan ratio in the examples presented here indicated that in PtAF hearts $82.2 \pm 16.1\%$ of the PSs formed I-filament ASWs. However, in the NHs, only $33.5 \pm 8.4\%$ of PSs evolved in such a way. Importantly, the meandering trajectories of most ASWs' filaments in PtAF hearts were confined to either the thinnest, largely translucent LAA regions or to the immediate vicinity of such regions. Rarely did some of the ASWs' trajectories extend into thick pectinate muscles of the LAA (see heart 2 in *Figure 5B*). *Figure 5C* and *D* summarizes the large differences in AF dynamics between the two groups of hearts. *Figure 5C* compares the lifespan of I-filament ASWs in terms of number of rotations. Clearly, while in NHs I-filament, ASWs never lasted more than three rotations, we found examples of I-filament ASWs lasting six rotations or more in 12/16 movies from PtAF hearts . As shown in *Figure 5D*, in a subset of four animals, the average number of BTs was significantly larger in normal than in PtAF hearts.

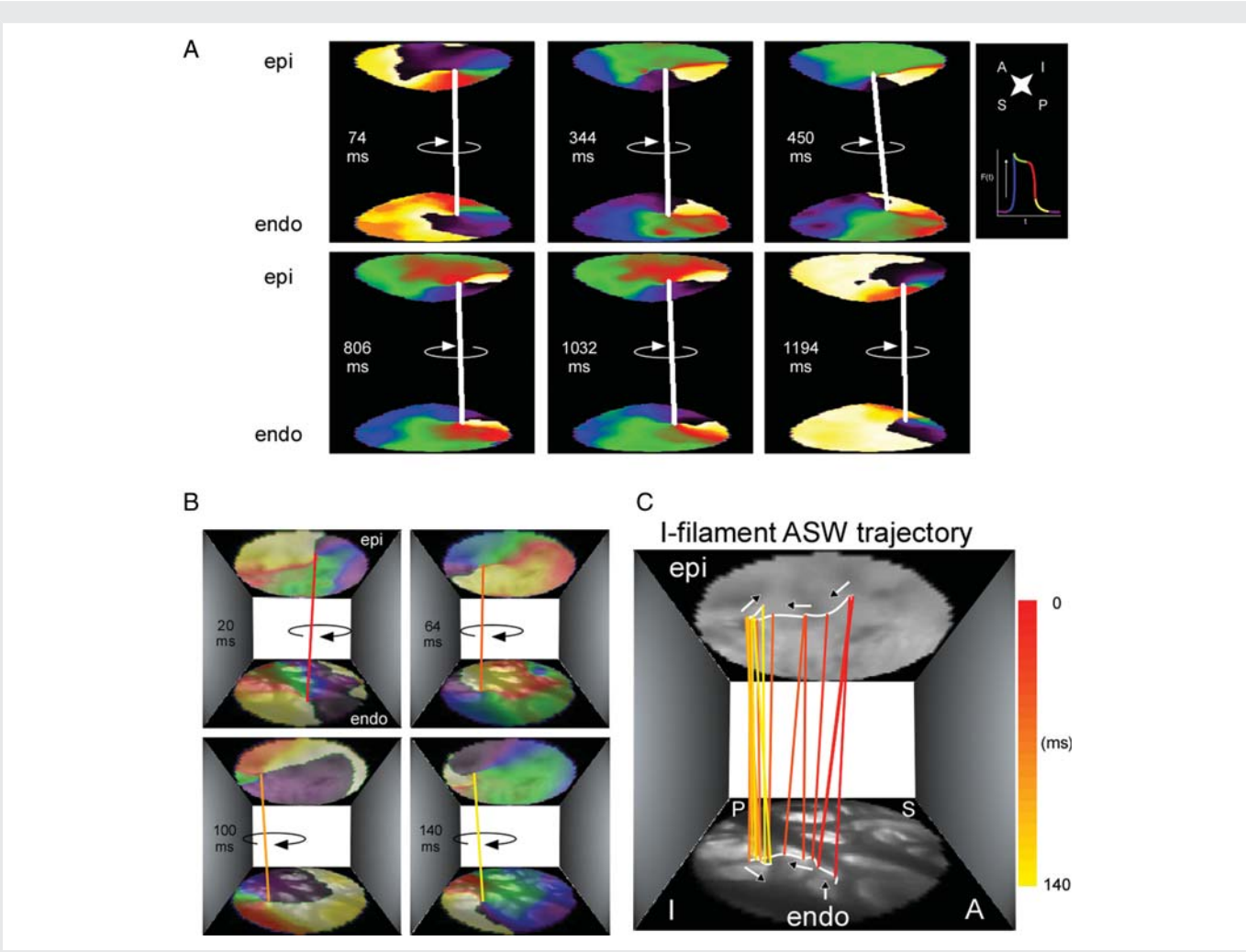

Figure 4 I-filament ASWs in a PtAF heart. (*A*) Representative sequential colour phase maps of a reconstructed ASW spanning the anterior LAA wall. The white line joining the epicardial and endocardial singularity points indicates the presence of a sustained ASW whose I-shaped filament rotates clockwise during 1120 ms. (*B*) Meandering trajectory of an ASW filament during one rotation lasting 140 ms. Sequential colour phase maps and corresponding filament locations superimposed with matching real images of the endocardial and epicardial surfaces. (*C*) Tracing the filament trajectory. From 20 to 64 ms, the filament remained anchored to in thin myocardium bordered by thick pectinate muscles. Between 64 and 140 ms, the filament drifted across a pectinate muscle segment before anchoring to a neighbouring island of thin myocardium. Phase map colours as in *Figure 1*.

3.5 Local action potential duration and apparent conduction velocity

Supplementary material online, *Table S1* summaries the quantification of action potential duration (APD) and apparent conduction velocity (ACV) at the thinnest and thickest myocardial regions of the LAA. ACV at the CL of 200 and 300 ms was significantly lower in PtAF hearts than NHs at the thickest atrial regions. Similarly, APD90 at 300 ms CL was significantly shorter in PtAF than NHs at the thickest atrial regions. Altogether, the wavelength at the several locations, calculated as Wave length (WL) = APD × ACV, was significantly shorter in PtAF than in NHs.

3.6 Numerical simulations

As illustrated in *Figure 6A–C*, we initiated ASW using an S1–S2 protocol and studied the filament dynamics in the absence and the presence of heterogeneously distributed stretch. We compared the results in control (NH condition) with those after ionic remodelling secondary to changes in either three or four major ionic conductances as previously reported (PtAF-3 currents and PtAF-4 currents).[15] As illustrated in *Figure 6C*, in the absence of stretch, simulated ASWs drifted continuously with their filament inscribing a flowery pattern around the interface between thin and thick regions. In a similar experiment with inverted geometry (i.e. thick region in the periphery), the filament also circumnavigated the boundary between thin and thick regions (see Supplementary material online, *Figure S3*), which demonstrated that the drifting behaviour was independent of boundary conditions. We then compared filament dynamics in terms of the meandering angle α (*Figure 6C*) in the presence and the absence of heterogeneous stretch. *Figure 6D* clearly shows that while ionic remodelling alone increased the amount of meandering, stretch significantly reduced meandering in all cases, regardless of the experimental condition (i.e. normal; PtAF-3 currents; PtAF-4 currents). However, as shown in *Figure 6E*, the stabilizing effect of

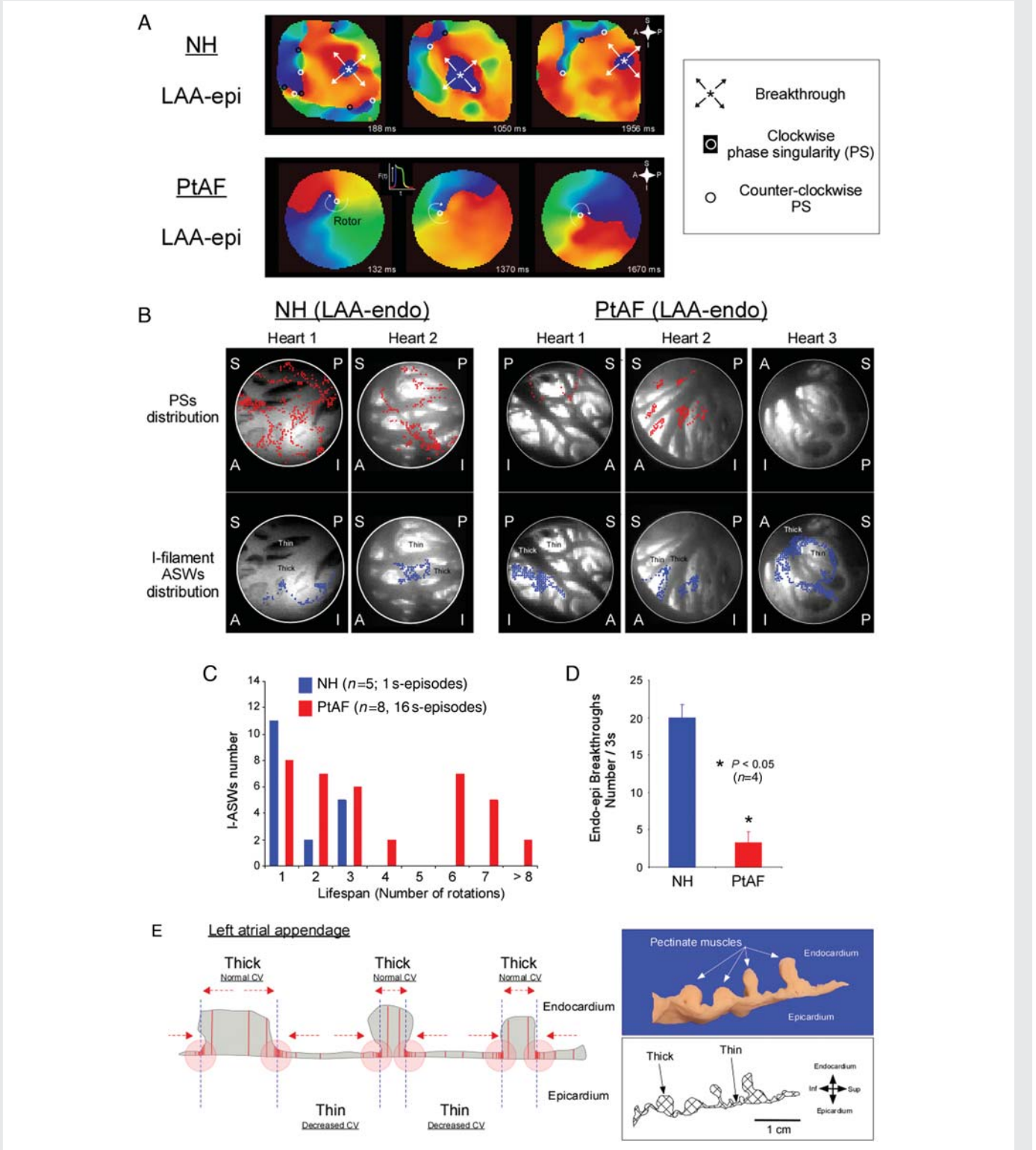

Figure 5 AF dynamics in normal and PtAF hearts. (*A*) Representative sequential LAA-epi phase maps obtained from NH and PtAF hearts over a time window ~1 s. In the NH (top), the dynamics were characterized by BTs and multiple PSs of both chiralities. In the PtAF heart (bottom), a sustained ASW was seen rotating clockwise throughout the recording period. Phase movies colours as in *Figure 1*. Inset; key for the various dynamic components. (*B*) Anatomical distribution of transient PSs (red dots, top) and I-filament ASWs lasting >3 rotations (blue dots, bottom) on the LAA-endo in two NH and three PtAF hearts. The PSs were transient in NH. In PtAF hearts, most PSs evolved into I-filament ASWs which meandered within the thin atrial myocardium or around thin-to-thick interfaces. S, superior; I, inferior; A, anterior; P, posterior. (*C*) Histogram of I-ASW's rotation numbers at the LAA in NH and PtAF. (*D*) Average number of BTs in NH and PtAF hearts. (*E*) Heterogeneous walls of LAA are substrates for scroll wave meandering. See text for details.

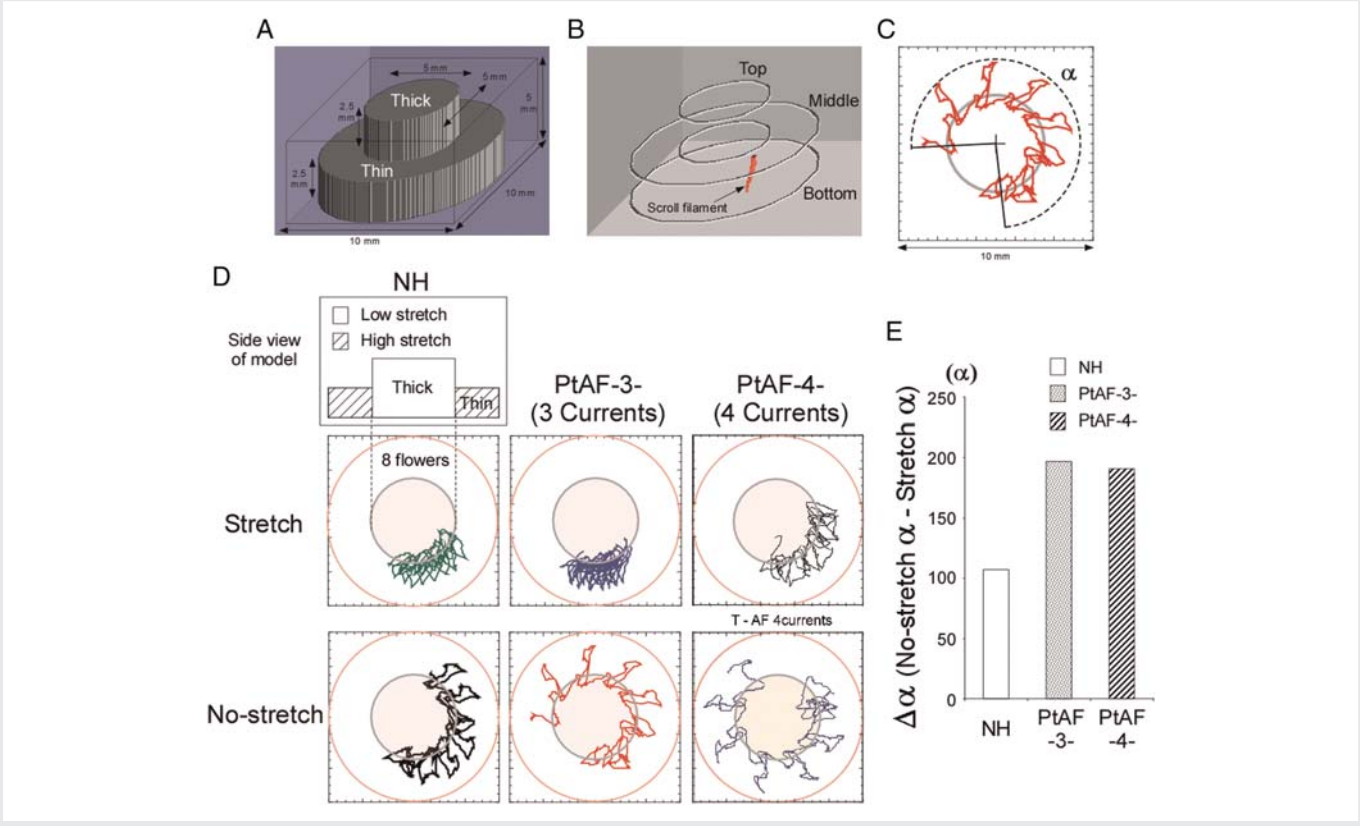

Figure 6 Numerical simulation: mechanism of scroll filament meandering during AF. (*A*) Diagram illustrating the spatial dimensions of the atrial model. (*B*) Snapshot of 3D simulation movie. Red, scroll wave filament. (*C*) Quantification of filament trajectory using α as the meandering angle. (*D*) Schematic of simulated atrial models, trajectories, and relative rates of filament meandering over eight petals/1 s of SW meandering. (*E*) Plot of Δα in NH, PtAF-3, and PtAF-4: angular meandering of filament decreases under conditions of heterogeneous stretch.

heterogeneous stretch, measured as Δα, was substantially larger under both conditions of ionic remodelling than in the normal case. Finally, we examined in detail the time spent by ASW filaments in the thin vs. thick regions of the 3D geometry. As shown in Supplementary material online, *Figure S4*, in all cases, most of the filaments' time was spent in the thin region regardless of the presence or the absence of stretch, although stretch appreciably increased the difference in PtAF conditions.

4. Discussion

The most important results presented here are as follows: (i) 3D stretch-related AF dynamics are different in normal vs. PtAF hearts. In the former, ASWs are short-lived and interact repeatedly with focal BTs and incoming wavefronts from outside the optical field; in the latter, ASWs are more numerous and long-lasting, and are widely distributed throughout both atria. (ii) In both NH and PtAF hearts, ASWs form and meander around regions of sharp transition in myocardial thickness, but ASWs tend to be more stable in PtAF hearts. (iii) As shown numerically, ionic remodelling alone increases meandering, whereas combined ionic remodelling and increased stretch-activated channel conductance in thin regions forces ASW to stabilize within regions having large gradients in myocardial thickness.

4.1 Atrial SWs, mechanism of AF maintenance during PtAF

In PtAF patients structural and ionic remodelling of the atria are thought to contribute to AF perpetuation.[2,20] However, it is unclear how the 3D structure of the remodelled atria contributes to AF maintenance. Previously, pectinate muscles were suggested to cause electrical heterogeneities such as endocardium–epicardium dissociation leading to AF perpetuation.[21–24] Yet, a comprehensive evaluation of 3D AF dynamics in remodelled atria had not been conducted. The results presented here demonstrate that the dynamics of 3D wave propagation during stable AF are significantly different in normal vs. PtAF hearts. This strongly indicates that while the electrophysiological mechanism of AF maintenance may include 3D reentry in both cases, remodelling modifies the atrial substrate in such a way as to displace the reentrant sources away from the posterior wall into other regions of the atria and to make them more stable. Previous experimental and clinical studies have invoked various AF maintenance mechanisms, including reentry, spontaneous focal discharges, and multiple wavelets. While reentrant mechanisms have proved to be central for AF maintenance,[25] we recently demonstrated an interplay between reentry and spontaneous focal discharges during stretch-related AF.[9] We suggested that reentry might either terminate and/or be re-initiated by a spontaneous focal discharge in the vicinity of the reentry core. In addition, Eckstein *et al.*[26] suggested that pronounced dissociation of electrical activity occurs between the

epicardial layer and the endocardial bundle network and correlates with increasing stability and complexity of the AF substrate. The data presented here suggest that in remodelled atria, reentrant mechanisms in the form of ASWs are more prevalent and last longer than in the NHs. They suggest also that more than one ASWs of similar frequency coexisted in the LA and RA to maintain the fibrillatory activity. In fact, remodelling significantly reduced the frequency gradient within the atria in PtAF compared with NHs. Thus, we recognize that during PtAF two or more ASWs may coexist to maintain AF.

4.2 Atrial wall thickness and ASWs' filament tension

Our simulations predict that gradients in myocardial thickness are responsible for gradients in stretch-activated channel activity and that both gradients are the main determinant of scroll wave dynamics. We thus propose that heterogeneity in myocardial thickness while intra-atrial pressure is constant leads to a differential sarcomere lengthening in thick and thin regions which in turn activates stretch-activated channels heterogeneously. Such heterogeneities-exquisitely located at the transition thick-to-thin myocardium are likely to be sites at which SWs filaments stabilize. The importance of the scroll wave filament tension as a determinant of scroll wave stability was previously demonstrated *in silico* as well as in experiments in heterogeneous chemical excitable media.[18,27,28] Under conditions of normal excitability, the filament is submitted to a 'positive tension' that forces it to shrink, and therefore to drift towards the thinnest portions of the medium.[27] In contrast, in conditions of low excitability, the filament tension becomes negative, and therefore the filament may grow in length, become unstable and rapidly drift towards and terminate in the thickest portion of the medium.[29,30] Moreover, in theory, sharp transitions between thin and thick excitable media should favour scroll wave formation and anchoring.[13] Such numerical predictions are consistent with our experimental results showing that the heterogeneous atrial architecture forces ASWs to drift towards the thinnest regions. Our data further show that during AF, ASWs form and linger around interfaces between thin and thick atrial muscle regions, presumably because of opposing drifting influences exerted by the two regions. As presented in *Figure 5E* and also in Supplementary material online, *Table S1*, the conduction velocity was markedly decreased (about 30%) in the thinnest regions. We propose that this was likely to prevent ASWs from drifting into the thick regions where filaments experience greater instability. We reported previously[31] that when an impulse propagates from a thin (e.g. one of the PVs) into a thick region (e.g. the PLA), electrical source-to-sink mismatch leads to propagation delays, wavebreak, and ASWs formation. Here, we demonstrate that most ASWs meander and/or stabilize at large gradients in myocardial thickness. Previously, Wu *et al.*[24] indicated that pectinate muscle ridges are sites of electrical source-to-sink mismatch where wavebreaks often occur, resulting in spiral wave attachment. The present work confirms these findings as exemplified by *Figure 5* showing a high propensity for wavebreak formation, where pectinate muscles merge with the atrial wall. Besides, our results provide an explanation for the maintenance of reentrant sources in such locations. We propose that the 3D dynamics of atrial SWs in the presence of heterogeneous myocardial thickness and stretch results in SWs anchoring in regions of increased thickness gradients.

4.3 Stretch contributes to ASWs stabilization

Our experiments indicate that in PtAF hearts, ASWs tend to stabilize at the edges of pectinate muscles. The simulations confirm that filament meandering tends to be confined to myocardial thickness interfaces, and demonstrate that, while ionic remodelling alone increases the rate of drift, the addition of stretch greatly decreases the filament angular meandering and leads to ASWs stabilization (*Figure 6D* and *E*). Such predictions agree well with the significantly increased ASW filament lifespan in PtAF hearts, in which several ASWs lasted for six rotations or more (*Figure 5C*). Interestingly, ASW stabilization did not correlate with the decreased APD and WL that are characteristic of remodelling in PtAF hearts. APD shortening has been previously associated with a decreased meandering in 2D simulations in the absence of stretch.[15] However, our results demonstrate that heterogeneity in muscle thickness supersedes the ionic remodelling effect and contributes to scroll wave meandering along large thickness gradients. Then, atrial dilatation and heterogeneous stretch provide additional conductances that force ASWs to stabilize (*Figure 6*; see Supplementary material online, *Figure S1*). In this setting, it is likely that unbalanced source-to-sink relationships, produced by uneven stretch-activated ion channel conductances in thin vs. thick portions of the myocardial wall, significantly contributed to decrease ASW filament meandering. Thus, we propose that heterogeneous thickness and stretch together with ionic remodelling predispose to ASW stabilization.

4.4 Clinical implications

Altogether, the data agree with clinical findings indicating that the atrial architecture plays a critical role in establishing the substrate for both paroxysmal and persistent AF maintenance. In addition, the results provide a feasible mechanism by which the 3D atrial architecture of the human remodelled atria may favour ASW stabilization and perpetuation. They show also that in the electrically remodelled, dilated atria one or several relatively stable reentrant sources stabilize at interfaces between thick and thin muscle. Such a different behaviour helps explain the large difference in AF ablation outcomes in paroxysmal vs. persistent AF.[5] Obviously, additional factors are likely to contribute to such different outcomes. One major candidate is structural remodelling and its manifestation as fibrosis, which has not been considered here and must be evaluated in future studies.

4.5 Limitations

Because of technical limitations, electrophysiological and haemodynamical measurements *in vivo* as well as an evaluation of autonomic remodelling were not obtained. Also, interstitial fibrosis might have played an important role in ASW dynamics. While we measured an increased percentage of interstitial fibrosis in the LAA of remodelled hearts vs. NHs (data not shown), we did not evaluate the relationship between interstitial fibrosis distribution and ASW location. In terms of spiral wave dynamics in 2D, we have recently emphasized that the percentage as well as the distribution of fibrotic patches are of paramount importance.[32] A definitive experimental proof of our proposed mechanisms of AF maintenance would be to show that an electrical gradient is induced by heterogeneous stretch-activated channel activation. We thus recognize that this aspect of ASW dynamics, as well as the effect of SACs blockers in PtAF hearts will have to be investigated in future works. Recently, Cha *et al.* have

demonstrated that IKH are upregulated in atrial tachypaced AF.[33] Nevertheless, these are not considered in our simulations. Also, our numerical model did not account for variations in fibre direction expected with changes in myocardial thickness.

Besides, our wave pattern analysis of simultaneous BT numbers might have been (i) overestimated (up to 20% in each group) as we tolerated an endocardial–epicardial onset delay of up to 12 ms or (ii) oppositely underestimated as very slow conduction might have allowed waves originating at the same intra-myocardial location to be categorized as non-simultaneous. Our main conclusion, however, is unaffected. In addition, one likely explanation for the absence of DF increase in PtAF vs. NHs could be that our window of observation did not include other atrial sites that might have been activated at faster rates. In that eventuality, our conclusions would only relate to local conditions and not to impulse propagation properties and mechanisms in the rest of the substrate, as presented in the more comprehensive study by Eckstein *et al.*[26] Also centrifugal BT waves may relate to transmural propagation of fibrillatory waves as elegantly shown in de Groot *et al.*[34] to focal discharges, or else to the manifestation of an intra-mural reentrant activity. Also, proofs of reentrant activities in the human atrium are still lacking while a multiple wavelets mechanism has been presented in a previous study.[35]

Supplementary material

Supplementary material is available at *Cardiovascular Research* online.

Acknowledgements

We thank Dr José Jalife for his suggestions and support. We thank Jiang Jiang and Wei Zhang for technical support.

Conflict of interest: none declared.

Funding

This work was supported by NHLBI grants (PO1 HL039707, PO1 HL087226, and RO1 HL070074 to J.J.; RO1-HL087055, to J.K.) and ACCF/GE Healthcare Career Development Award to J.K; Heart Rhythm Society Fellowship Award, The Fellowship of Japan Heart Foundation/The Japanese Society of Electrocardiology to M.Y.

References

1. Camm AJ, Kirchhof P, Lip GY, Schotten U, Savelieva I, Ernst S *et al*. Guidelines for the management of atrial fibrillation: the Task Force for the Management of Atrial Fibrillation of the European Society of Cardiology (ESC). *Eur Heart J* 2010;**31**:2369–2429.
2. Wijffels MC, Kirchhof CJ, Dorland R, Allessie MA. Atrial fibrillation begets atrial fibrillation. A study in awake chronically instrumented goats. *Circulation* 1995;**92**: 1954–1968.
3. Benjamin EJ, Levy D, Vaziri SM, D'Agostino RB, Belanger AJ, Wolf PA. Independent risk factors for atrial fibrillation in a population-based cohort. The Framingham Heart Study. *JAMA* 1994;**271**:840–844.
4. Yoshida K, Ulfarsson M, Oral H, Crawford T, Good E, Jongnarangsin K *et al*. Left atrial pressure and dominant frequency of atrial fibrillation in humans. *Heart Rhythm* 2011;**8**: 181–187.
5. Sanders P, Berenfeld O, Hocini M, Jais P, Vaidyanathan R, Hsu LF *et al*. Spectral analysis identifies sites of high-frequency activity maintaining atrial fibrillation in humans. *Circulation* 2005;**112**:789–797.
6. Sanchez JE, Kay GN, Benser ME, Hall JA, Walcott GP, Smith WM *et al*. Identification of transmural necrosis along a linear catheter ablation lesion during atrial fibrillation and sinus rhythm. *J Interv Card Electrophysiol* 2003;**8**:9–17.
7. Kalifa J, Klos M, Zlochiver S, Mironov S, Tanaka K, Ulahannan N *et al*. Endoscopic fluorescence mapping of the left atrium: a novel experimental approach for high resolution endocardial mapping in the intact heart. *Heart Rhythm* 2007;**4**:916–924.
8. Council IoLARCoLSNR. *Guide for the care and use of laboratory animals*. Washington, DC: National Academy Press; 1996. p1–140.
9. Yamazaki M, Vaquero LM, Hou L, Campbell K, Zlochiver S, Klos M *et al*. Mechanisms of stretch-induced atrial fibrillation in the presence and the absence of adrenocholinergic stimulation: interplay between rotors and focal discharges. *Heart Rhythm* 2009; **6**:1009–1017.
10. Skanes AC, Mandapati R, Berenfeld O, Davidenko JM, Jalife J. Spatiotemporal periodicity during atrial fibrillation in the isolated sheep heart. *Circulation* 1998;**98**: 1236–1248.
11. Gray RA, Pertsov AM, Jalife J. Spatial and temporal organization during cardiac fibrillation. *Nature* 1998;**392**:75–78.
12. Warren M, Guha PK, Berenfeld O, Zaitsev A, Anumonwo JM, Dhamoon AS *et al*. Blockade of the inward rectifying potassium current terminates ventricular fibrillation in the guinea pig heart. *J Cardiovasc Electrophysiol* 2003;**14**:621–631.
13. Pertsov AM. Three-dimensional Vortex-like Reentry. In: Zipes DP, Jalife J, ed. *From Cell to Bedside*. 3rd ed. Philadelphia, PA: WB Saunders; 2000. p403–410.
14. Courtemanche M, Ramirez RJ, Nattel S. Ionic targets for drug therapy and atrial fibrillation-induced electrical remodeling: insights from a mathematical model. *Cardiovasc Res* 1999;**42**:477–489.
15. Pandit SV, Berenfeld O, Anumonwo JM, Zaritski RM, Kneller J, Nattel S *et al*. Ionic determinants of functional reentry in a 2-D model of human atrial cells during simulated chronic atrial fibrillation. *Biophys J* 2005;**88**:3806–3821.
16. Kamkin A, Kiseleva I, Wagner KD, Bohm J, Theres H, Gunther J *et al*. Characterization of stretch-activated ion currents in isolated atrial myocytes from human hearts. *Pflugers Arch* 2003;**446**:339–346.
17. Lazar S, Dixit S, Marchlinski FE, Callans DJ, Gerstenfeld EP. Presence of left-to-right atrial frequency gradient in paroxysmal but not persistent atrial fibrillation in humans. *Circulation* 2004;**110**:3181–3186.
18. Winfree AT, Strogatz SH. Organizing centres for three-dimensional chemical waves. *Nature* 1984;**311**:611–615.
19. Pertsov A, Aliev P, Krinsky V. Three-dimensional twisted vortices in an excitable chemical medium. *Nature* 1990;**345**:419–421.
20. Nattel S, Maguy A, Le Bouter S, Yeh YH. Arrhythmogenic ion-channel remodeling in the heart: heart failure, myocardial infarction, and atrial fibrillation. *Physiol Rev* 2007; **87**:425–456.
21. Derakhchan K, Li D, Courtemanche M, Smith B, Brouillette J, Page PL *et al*. Method for simultaneous epicardial and endocardial mapping of in vivo canine heart: application to atrial conduction properties and arrhythmia mechanisms. *J Cardiovasc Electrophysiol* 2001;**12**:548–555.
22. Eckstein J, Verheule S, de Groot N, Allessie M, Schotten U. Mechanisms of perpetuation of atrial fibrillation in chronically dilated atria. *Prog Biophys Mol Biol* 2008;**97**: 435–451.
23. Schuessler RB, Kawamoto T, Hand DE, Mitsuno M, Bromberg BI, Cox JL *et al*. Simultaneous epicardial and endocardial activation sequence mapping in the isolated canine right atrium. *Circulation* 1993;**88**:250–263.
24. Wu TJ, Yashima M, Xie F, Athill CA, Kim YH, Fishbein MC *et al*. Role of pectinate muscle bundles in the generation and maintenance of intra-atrial reentry: potential implications for the mechanism of conversion between atrial fibrillation and atrial flutter. *Circ Res* 1998;**83**:448–462.
25. Jalife J, Berenfeld O, Mansour M. Mother rotors and fibrillatory conduction: a mechanism of atrial fibrillation. *Cardiovasc Res* 2002;**54**:204–216.
26. Eckstein J, Maesen B, Linz D, Zeemering S, van Hunnik A, Verheule S *et al*. Time course and mechanisms of endo-epicardial electrical dissociation during atrial fibrillation in the goat. *Cardiovasc Res* 2011;**89**:816–824.
27. Wellner M, Berenfeld O, Jalife J, Pertsov AM. Minimal principle for rotor filaments. *Proc Natl Acad Sci USA* 2002;**99**:8015–8018.
28. Zaritski RM, Mironov SF, Pertsov AM. Intermittent self-organization of scroll wave turbulence in three-dimensional excitable media. *Phys Rev Lett* 2004;**92**:168302.
29. Biktahsev VN, Holden AV, Zhang H. Tension of organizing filaments of scroll waves. *Phil Trans R Soc Lond A* 1994;**347**:611–630.
30. Rusakov A, Medvinsky AB, Panfilov AV. Scroll waves meandering in a model of an excitable medium. *Phys Rev E Stat Nonlin Soft Matter Phys* 2005;**72**:022902.
31. Klos M, Calvo D, Yamazaki M, Zlochiver S, Mironov S, Cabrera JA *et al*. Atrial septopulmonary bundle of the posterior left atrium provides a substrate for atrial fibrillation initiation in a model of vagally mediated pulmonary vein tachycardia of the structurally normal heart. *Circ Arrhythm Electrophysiol* 2008;**1**:175–183.
32. Tanaka K, Zlochiver S, Vikstrom KL, Yamazaki M, Moreno J, Klos M *et al*. The spatial distribution of fibrosis governs fibrillation wave dynamics in the posterior left atrium during heart failure. *Circ Res* 2007;**101**:839–847.
33. Cha TJ, Ehrlich JR, Chartier D, Qi XY, Xiao L, Nattel S. Kir3-based inward rectifier potassium current: potential role in atrial tachycardia remodeling effects on atrial repolarization and arrhythmias. *Circulation* 2006;**113**:1730–1737.
34. de Groot NM, Houben RP, Smeets JL, Boersma E, Schotten U, Schalij MJ *et al*. Electropathological substrate of longstanding persistent atrial fibrillation in patients with structural heart disease: epicardial breakthrough. *Circulation* 2010;**122**: 1674–1682.
35. Allessie MA, de Groot NM, Houben RP, Schotten U, Boersma E, Smeets JL *et al*. Electropathological substrate of long-standing persistent atrial fibrillation in patients with structural heart disease: longitudinal dissociation. *Circ Arrhythm Electrophysiol* 2010;**3**: 606–615.